Dynamic analysis of multiple-photon optical processes in semiconductor quantum dots

2006 J. Phys.: Condens. Matter 18 9071

(http://iopscience.iop.org/0953-8984/18/39/033)

INSTITUTE OF PHYSICS PUBLISHING JOURNAL OF PHYSICS: CONDENSED MATTER

J. Phys.: Condens. Matter **18** (2006) 9071–9082 doi:10.1088/0953-8984/18/39/033

Dynamic analysis of multiple-photon optical processes in semiconductor quantum dots

Y Fu, T-T Han, Y Luo and H Ågren

Department of Theoretical Chemistry, School of Biotechnology, Royal Institute of Technology, AlbaNova, S-106 91 Stockholm, Sweden

Received 15 May 2006, in final form 4 August 2006
Published 15 September 2006
Online at stacks.iop.org/JPhysCM/18/9071

Abstract

Semiconductor quantum dots (QDs) have been gaining much attention because of their outstanding properties for multiple-photon microscopy applications. By solving nonperturbatively the time-dependent Schrödinger equation, it has been shown that the large number of energy states densely compacted in both the conduction and valence bands of the QD greatly enhance the inter-band and intra-band optical couplings between two energy states induced by multiple photons from ultra-fast and ultra-intense lasers. The multiphoton absorption processes are further enhanced by many energy relaxation processes in commonly used semiconductors, which are generally represented by the relaxation energy in the order of tens of meV. Numerical calculation of multiphoton processes in QDs agrees with experimental demonstration. After proper designing, QDs can be activated by infrared radiation to emit radiation in the visible optical regime (up-conversion) for bioimaging applications.

1. Introduction

The multiphoton excitation process has a great number of unique advantages over one-photon excitation in biological and medical studies, such as reduced specimen photodamage and enhanced penetration depth, localization of excitation, which results in a better imaging resolution, reduced photobleaching, and the ability to trigger local photochemical reaction [1–3]. Semiconductor quantum dots (QDs) are highly fluorescent, and have captivated the interest of the biomedical community as the ultimate tags for cellular imaging, because of the better photochemical stability, extreme brightness, broad excitation spectral range and narrow and symmetric emission spectrum, which is independent of excitation frequency [4–6]. A record high two-photon cross section was reported from water-soluble semiconductor quantum dots [7].

As indicated by Lami *et al* [8], two-photon absorption has been widely studied in a large variety of materials under a broad spectrum of physical conditions since its prediction by Goeppert-Mayer [9] and the first observation by Kaiser and Garret [10]. The multiphoton process has largely been treated theoretically by steady-state perturbation approaches, e.g.,

the scaling rules of multiphoton absorption by Wherrett [11] and the analysis of two-photon excitation spectroscopy of CdSe nanocrystals by Schmidt *et al* [12].

In multiphoton microscopy, a laser is focused and raster-scanned across the sample. Focusing alone is not enough to make two-photon microscopy practical. A pulsed laser is normally used to increase further the probability of optical coupling with the electrons inside the QD, while still keeping the average power relatively low. The full width at half maximum of laser pulses used by Blanton *et al* was 1 ps [13]. It was only 140 fs by Klimov and McBranch when studying ultrafast dynamics in CdSe nanocrystals [14, 15]. The peak power of the ultrashort laser pulse can be as high as 30 GW cm^{-2} [13]. Under the present circumstances, the steady-state perturbation theory is not valid. In this work we study the dynamic properties of multiphoton optical processes in semiconductor QDs by solving nonperturbatively the time-dependent Schrödinger equation.

2. Theoretical considerations

2.1. One-electron Hamiltonian of the quantum dot

We consider the one-electron Hamiltonian of a quantum dot in the form of [16–18]

$$H_n = -\frac{\hbar^2\nabla^2}{2m_n^*} + V_n(\boldsymbol{r}), \qquad V_n(\boldsymbol{r}) = \begin{cases} -\Delta_n & b \leqslant 1 \\ 0 & \text{otherwise} \end{cases} \tag{1}$$

for conduction-band electrons; m_n^* is the effective mass of the electron. $b = (x^2 + y^2 + z^2)/a^2$, a is the radius of the quantum dot. Δ_n is the conduction-band offset between the quantum dot and the surrounding medium. When referring to vacuum, $\Delta_n = \chi$, which is the electron affinity of the material surface. Similar expressions can be written down for the valence-band holes. Here the conduction-band electrons and valence-band holes are described using the effective mass approximation (EMA) [16–21]. For wurtzite CdS under the current theoretical analysis, the energy bandgap is $E_g = 2.485$ eV, the quantum confinement $\Delta_c = 4.79$ eV for conduction-band electrons and $\Delta_v = 2.21$ eV for valence-band holes, electron and hole effective masses are $m_c^* = 0.2\ m_0$ and $m_v = 0.53\ m_0$, respectively, m_0 is the electron rest mass, the high-frequency dielectric constant $\epsilon_\infty = 5.32$, and the energy related to the optical transition matrix $E_p = 20.7$ eV [17, 21–29]. Figure 1 shows the schematic energy band structure of the CdS QD under investigation, where E_{c0} denotes the ground sublevel ('0') in the conduction band (c) and E_{c1} is the first excited sublevel. E_{v0} and E_{v1} are ground and first excited sublevels in the valence band.

Advanced theories to account for the fine structures in the energy bands of II–VI semiconductor nanocrystals have been developed, e.g. the effective bond-orbital model for valence-band holes [30, 31], the valence-band mixing effect [32], the sp^3s^* semi-empirical tight-binding theory [24, 25, 33], and the sp^3d^5 nearest-neighbour tight-binding model [29, 34]. Since the QD of interest consists of 10^5 atoms, the general principal features of the optical spectrum are expected to be determined by the geometric structures of the quantum dot; we apply the EMA theory to describe the electronic and optic properties of the QDs. It was shown that the ground level energies obtained from equation (1) are very close to the results from the sp^3d^5 nearest-neighbour tight-binding model [35].

For conduction-band electrons described by equation (1), the eigenfunctions of the Schrödinger equation (equation (1)) are expressed in the form of $\psi_{\ell m}(r, \theta, \phi) = R_\ell(r)Y_{\ell m}(\theta, \phi)$, where $Y^*_{\ell m}(\theta, \phi)$ is the angular momentum eigenfunction, and the radial function is expressed by spherical Bessel and Neumann functions [36]. Figures 2(a) and (b) show the energy states in a CdS QD having a radius of 3.7 nm. Notice that such a CdS QD has a total of 319 bound levels ($E < 0$) in the conduction band. We include a total of 10 000 states

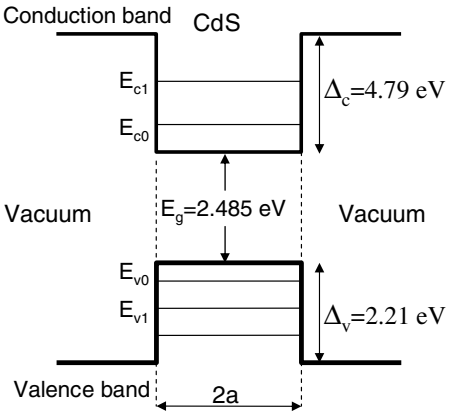

Figure 1. Schematic energy band structure of the CdS QD embedded in vacuum.

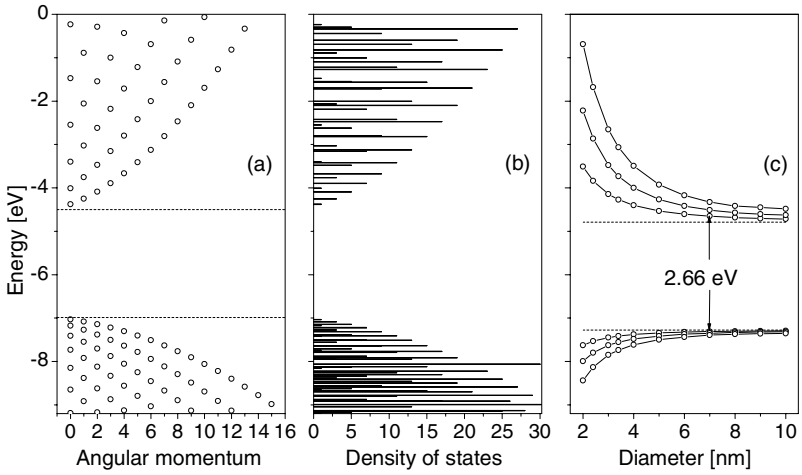

Figure 2. (a) Confined energy states in a CdS QD having a radius of $a = 3.7$ nm. (b) Density of confined states. (c) Energy sublevels as functions of the diameter ($2a$) of the CdS QD.

in the intraband optical transition calculations, where the continuum states extend to 10.0 eV at a step of 10 meV and $l \in (0, 5)$. It was shown that taking into account only a limited number of intermediate states gives rise to a numerical problem [37, 38] (see more discussions below about the gauge invariance). The relationship between the energy sublevels in the CdS QD and the diameter of the QD is presented in figure 2(c), where we observe that the separation between the ground sublevels in the conduction and valence bands increases when the QD diameter decreases. This is one of the important advantages offered by the semiconductor QDs for multiphoton bioimaging [6].

2.2. Electron–photon interaction

Denoting $\boldsymbol{A}$ as the vector potential of the electromagnetic field, the Hamiltonian describing an electron with charge $-e$ in this field is

$$H = \frac{(\boldsymbol{p} + e\boldsymbol{A})^2}{2m_0} - e\phi + V(\boldsymbol{r}) \tag{2}$$

where $\boldsymbol{p}$ is the electron momentum and ϕ is the scalar potential of the electromagnetic field. Consider the kinetic energy

$$\frac{\boldsymbol{p}^2}{2m_0} + \frac{e\boldsymbol{A}\cdot\boldsymbol{p}}{2m_0} + \frac{e\boldsymbol{p}\cdot\boldsymbol{A}}{2m_0} + \frac{e^2\boldsymbol{A}^2}{2m_0} \tag{3}$$

and the following ratios:

$$\left|\frac{e\boldsymbol{A}\cdot\boldsymbol{p}}{\boldsymbol{p}^2}\right| \approx \left|\frac{e^2\boldsymbol{A}^2}{e\boldsymbol{A}\cdot\boldsymbol{p}}\right| \approx \frac{eA}{p}. \tag{4}$$

Moreover [39, 40]

$$\langle A^2\rangle = \frac{\hbar n_{\hbar\omega}}{2\epsilon\omega} \tag{5}$$

where $\hbar\omega$ is the photon energy and $n_{\hbar\omega}$ is the photon density. For an electron kinetic energy of 0.137 eV (the conduction-band ground state measured from the conduction-band edge of CdS), it is easy to obtain that $eA/p = 1.6\times10^{-7}$ when the optical power of the electromagnetic field is $S = 1.0\,\mathrm{W\,cm^{-2}}$, where S is the time-averaged amplitude of the Poynting vector representing the optical power of an electromagnetic field,

$$S = n_{\hbar\omega}\hbar\omega c \tag{6}$$

c is the speed of light, and the photon energy is 1.82 eV (the corresponding wavelength is 681 nm). Notice that $\langle A^2\rangle$ is proportional to the optical power so that $eA/p = 1.6\times10^{-5}$, which is still very small when the optical power is increased to $10^4\ \mathrm{W\,cm^{-2}}$. Therefore, the electron energy term containing $\boldsymbol{A}^2$ in equation (3) is very small as compared with the term linear in $\boldsymbol{A}$. However, the term containing $\boldsymbol{A}^2$ in equation (3) causes two-photon transitions between states of opposite parity when going beyond the dipole approximation [41]. Its contribution to the two-photon absorption was found to be negligible for optical transitions of silver atoms in NaCl:Ag [42]. For our CdS QD, we re-write the first-order perturbation in $\boldsymbol{A}^2$ as

$$\frac{eA^2}{2m_0}\mathrm{e}^{2\mathrm{i}(\boldsymbol{q}\cdot\boldsymbol{r}-\omega t)} \tag{7}$$

where the $\boldsymbol{q}$ is the optical wavevector. The optical wavelength is 681 nm when $\hbar\omega = 1.82$ eV so that the above perturbation is basically constant within the volume of a CdS QD, which does not induce optical transition between conduction-band and valence-band states. The total Hamiltonian of the electron in the electromagnetic field is therefore [40, 43]

$$H(\boldsymbol{r},t) = H_0(\boldsymbol{r}) + \frac{e}{m_0}\boldsymbol{A}\cdot\boldsymbol{p} \tag{8}$$

where H_0 is the Hamiltonian of the electron in the unperturbed quantum dot. In obtaining the last expression we have specified the gauge so that $\nabla\cdot\boldsymbol{A} = 0$ and $\phi = 0$. In the case where there is only one electron in the system $H_0 = H_n$, H_n is the one-electron Hamiltonian of equation (1).

Equation (8) is normally denoted as the velocity formula. It has been extensively studied that for systems containing nonlocal potential the length formula is the physically correct one for calculating the transition matrix for electric dipole processes [44, 45]. When using eigenstates of the unperturbed Hamiltonian as basis states, the results of the velocity formula become gauge dependent. In particular for two-level systems in the dipole approximation, this often results in pronounced differences between two formulae [45]. Only when taking a large number of states into account do both formulae give the same results, as requested by the gauge invariance [46–48]. We have included a total of 10 000 states in the intraband optical transition calculations to ensure the necessary gauge invariance.

By denoting $\boldsymbol{A} = A\boldsymbol{a}$, where $\boldsymbol{a}$ is the polarization unit vector of the optical field, $A(t)$ is given by [49]

$$A(t) = \begin{cases} 0 & t < 0 \\ \sqrt{\dfrac{\hbar}{2\omega\epsilon\Omega}}\left[b^{+}\mathrm{e}^{\mathrm{i}(\omega t+\boldsymbol{q}\cdot\boldsymbol{r})} + b\mathrm{e}^{-\mathrm{i}(\omega t+\boldsymbol{q}\cdot\boldsymbol{r})}\right] & t \geqslant 0 \end{cases} \tag{9}$$

b^{+} and b are creation and annihilation operators of the photon field; Ω is the normalization space volume. Here $t = 0$ is the time at which the optical field is switched on. As discussed earlier, one sets $\mathrm{e}^{\mathrm{i}\boldsymbol{q}\cdot\boldsymbol{r}} = 1$.

We denote the wavefunction of the total system composed of electrons and photons as

$$\Psi(\boldsymbol{r}, t) = \sum_j C_j(t)\psi_j(\boldsymbol{r})u_j \exp\left(-\mathrm{i}E_j t/\hbar\right)|N_{\hbar\omega}\rangle \tag{10}$$

where $|N_{\hbar\omega}\rangle$ describes the photon field with $N_{\hbar\omega}$ as the number of photons at energy $\hbar\omega$ ($n_{\hbar\omega} = N_{\hbar\omega}/\Omega$).

$$H_0(\boldsymbol{r})\psi_j(\boldsymbol{r}) = E_j\psi_j(\boldsymbol{r}) \tag{11}$$

describes the unperturbed electron system (again notice that H_0 is the Hamiltonian describing electrons in the QD). u_j is the lattice-periodic Bloch function. For conduction-band electrons it is denoted as u_{c}, and for valence-band holes it is u_{v}. It is easy to obtain the following equation for the wavefunction coefficient:

$$\begin{aligned}\mathrm{i}\hbar\frac{\mathrm{d}C_j(t)}{\mathrm{d}t} = {} & \frac{e}{m_0}\sqrt{\frac{\hbar}{2\omega\epsilon\Omega}}\sum_i\langle\psi_j(\boldsymbol{r})u_j|\boldsymbol{a}\cdot\boldsymbol{p}|\psi_i(\boldsymbol{r})u_i\rangle C_i(t) \\ & \times\left\{\sqrt{N_{\hbar\omega}}\exp\left[\frac{\mathrm{i}(E_j - E_i - \hbar\omega)t}{\hbar}\right] + \sqrt{N_{\hbar\omega}+1}\exp\left[\frac{\mathrm{i}(E_j - E_i + \hbar\omega)t}{\hbar}\right]\right\}\end{aligned} \tag{12}$$

by inserting equation (10) into the time-dependent Schrödinger equation. The term headed by $\sqrt{N_{\hbar\omega}}$ corresponds to the photon absorption, while the one with $\sqrt{N_{\hbar\omega}+1}$ is the photon emission.

When the optical power of the external light source is rather high so that it solely determines $N_{\hbar\omega}$, $N_{\hbar\omega} \approx N_{\hbar\omega} + 1$. In this case, equation (12) becomes

$$\begin{aligned}\mathrm{i}\hbar\frac{\mathrm{d}C_j(t)}{\mathrm{d}t} = {} & -\mathrm{i}\hbar\gamma_j C_j(t) + \frac{e}{m_0\omega}\sqrt{\frac{2S}{\epsilon c}}\sum_i\langle\psi_j(\boldsymbol{r})u_j|\boldsymbol{a}\cdot\boldsymbol{p}|\psi_i(\boldsymbol{r})u_i\rangle C_i(t) \\ & \times\exp\left[\frac{\mathrm{i}(E_j - E_i)t}{\hbar}\right]\cos(\omega t)\end{aligned} \tag{13}$$

by utilizing equation (6) and by considering the constant stream of the incident photons. Here we have included positive γ s to account phenomenologically for the relaxation of the system by following [50, 51].

The optical matrix element of interband transitions from the valence-band state to a conduction-band state is

$$\langle\psi_j u_{\mathrm{c}}|\boldsymbol{a}\cdot\boldsymbol{p}|\psi_i u_{\mathrm{v}}\rangle = \boldsymbol{a}\cdot\boldsymbol{p}_{\mathrm{cv}}\langle\psi_j|\psi_i\rangle = \boldsymbol{a}\cdot\boldsymbol{p}_{\mathrm{cv}}\delta_{\ell_j\ell_i}\delta_{m_j m_i}\int_0^\infty r^2\mathrm{d}r\; R^*_{\ell_j}(r)R_{\ell_i}(r) \tag{14}$$

where $\boldsymbol{p}_{\mathrm{cv}} = \langle u_{\mathrm{c}}|\boldsymbol{p}|u_{\mathrm{v}}\rangle$ is the momentum matrix element, $E_p = p_{\mathrm{cv}}^2/2m_0$.

Between two states within the same band (either the conduction band or the valence band), referred to as the intraband transition, the optical matrix element is

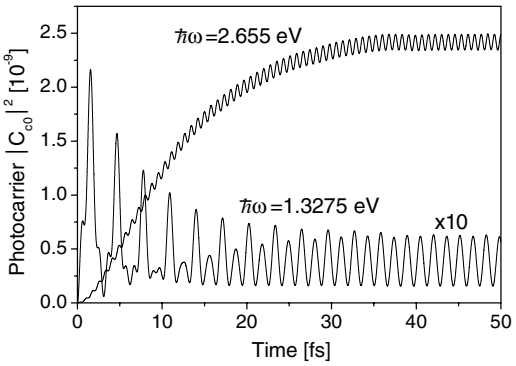

Figure 3. Temporal developments of the occupation of the conduction-band ground state $|C_{c0}(t)|^2$ induced by a CW excitation switched on at $t = 0$. $\hbar\omega$ is the photon energy of excitation radiation and an optical power $S = 100$ W cm^{-2}.

$$\langle\psi_j u_c|\boldsymbol{a}\cdot\boldsymbol{p}|\psi_i u_c\rangle = \langle\psi_j|\boldsymbol{a}\cdot\boldsymbol{p}|\psi_i\rangle = m_0\boldsymbol{a}\cdot\langle\psi_j|\frac{\mathrm{d}\boldsymbol{r}}{\mathrm{d}t}|\psi_i\rangle = \frac{\mathrm{i}m_0}{\hbar}\,\boldsymbol{a}\cdot\langle\psi_j|[H_0,\boldsymbol{r}]|\psi_i\rangle$$
$$= \frac{\mathrm{i}m_0(E_j-E_i)}{\hbar}\,\langle\psi_j|\boldsymbol{a}\cdot\boldsymbol{r}|\psi_i\rangle = \frac{\mathrm{i}m_0(E_j-E_i)}{\hbar}\int_0^\infty r^2\,\mathrm{d}r$$
$$\times\int_0^\pi \sin\theta\,\mathrm{d}\theta\int_0^{2\pi}\mathrm{d}\phi\; R^*_{\ell_j}(r)Y^*_{\ell_j m_j}(\theta,\phi)\boldsymbol{a}\cdot\boldsymbol{r}R_{\ell_i}(r)Y_{\ell_i m_i}(\theta,\phi). \tag{15}$$

Writing $\boldsymbol{r} = r\boldsymbol{r}_0$, where $\boldsymbol{r}_0$ is the unit vector, $\boldsymbol{a} = a_x\boldsymbol{x}_0 + a_y\boldsymbol{y}_0 + a_z\boldsymbol{z}_0$, and $\boldsymbol{x}_0$, $\boldsymbol{y}_0$ and $\boldsymbol{z}_0$ are unit vectors along the x-, y- and z-directions, respectively,

$$\boldsymbol{a}\cdot\boldsymbol{r}_0 = a_x\sin\theta\cos\phi + a_y\sin\theta\sin\phi + a_z\cos\phi$$
$$= \sqrt{\frac{4\pi}{3}}\left(\frac{-a_x+\mathrm{i}a_y}{\sqrt{2}}Y_{11} + a_zY_{10} + \frac{a_x+\mathrm{i}a_y}{\sqrt{2}}Y_{1\bar{1}}\right) \tag{16}$$

so that the angular integral in equation (15) involves

$$\int_0^\pi \sin\theta\,\mathrm{d}\theta\int_0^{2\pi}\mathrm{d}\phi\; Y^*_{\ell_j m_j}(\theta,\phi)Y_{1m}(\theta,\phi)Y_{\ell_i m_i}(\theta,\phi) \tag{17}$$

which can be analytically evaluated by using the addition theorem for spherical harmonics

$$Y_{\ell_1 m_1}(\theta,\phi)Y_{\ell_2 m_2}(\theta,\phi) = \sum_{\ell=|\ell_1-\ell_2|}^{\ell_1+\ell_2} C(\ell, m_1+m_2|\ell_1 m_1;\ell_2 m_2)Y_{\ell,m_1+m_2}(\theta,\phi). \tag{18}$$

In the above equation, $C(\ell m|\ell_1 m_1;\ell_2 m_2)$ are the Clebsch–Gordan coefficients, whose analytical expression can be obtained from [52, 53].

3. Temporal development of photocarrier distribution

Figure 3 shows the occupation of the conduction-band ground state $|C_{c0}(t)|^2$, where subscript 'c' denotes the conduction band and '0' the ground state (refer to figure 1). Here we have assumed that the confined states in the valence band are initially occupied and a continuous-wave (CW) excitation radiation is switched on at $t = 0$. Notice that the energy separation between the ground states in the conduction and valence bands is 2.67 eV in a spherical CdS QD having a radius of 3.7 nm.

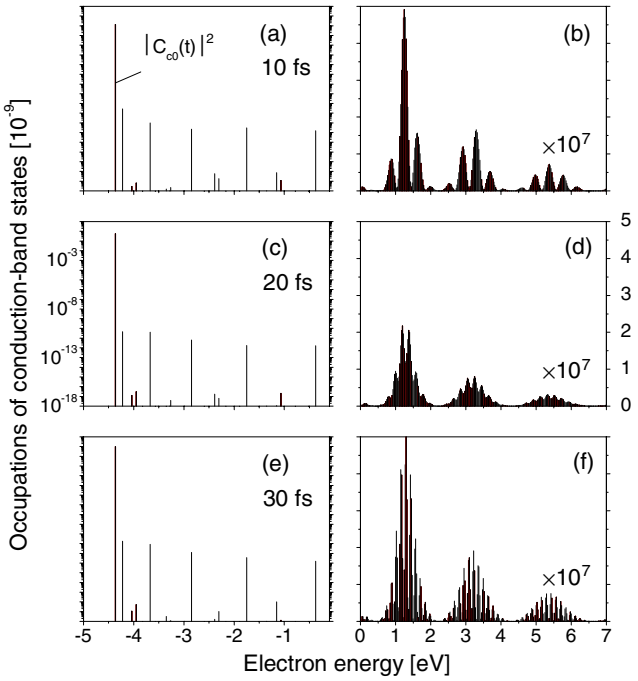

Figure 4. Photocarrier distribution in the conduction band after switching on a CW excitation radiation with a photon energy of 1.5 eV and an optical power of 50 W cm^{-2}. (a), (c), (e) confined states, (b), (d), (f) continuum states.

(This figure is in colour only in the electronic version)

Figure 4 shows the photogenerated carrier distribution in the conduction-band states, with a photon energy of $\hbar\omega = 1.5$ eV and an optical power of $S = 50$ W cm^{-2}. The sharp peak lines in the energy range below zero (confined sublevels) correspond to the occupations of the conduction sublevels of small ℓ values, largely originated from the ground sublevel in the valence band ($\ell = 0$). The first-stage excitation is from the ground sublevel in the valence band to sublevels of $\ell = 0$ in the conduction band, then the second-stage intraband transitions occur among sublevels of $\Delta\ell = \pm 1$ within the same conduction band; see figures 4(b), (d), and (f). The phenomenon is more profound in the continuum band of $E > 0$ because of the large density of states. When S is far below the order of GW cm^{-2}, the characteristics of the temporal developments of figures 3 and 4 are almost independent of the optical excitation power, while the density increases linearly with the optical excitation power.

It was experimentally demonstrated that fluorescence emission intensities from two-photon excited molecular fluorophores were proportional to the square of the excitation intensity with both pulsed and CW excitations [54]. For single-beam two-photon absorption (TPA), the differential equation describing the intensity of incident radiation along the z axis is given by [55]

$$\frac{\mathrm{d}S}{\mathrm{d}z} = -\alpha S - \beta S^2 \tag{19}$$

where α is the linear absorption coefficient and β is the TPA coefficient of the system. The TPA ability is also described by the TPA cross-section σ_2 of an individual molecule in the system, $\sigma_2 = \hbar\omega\beta/N$, where N is the number of molecules in the system.

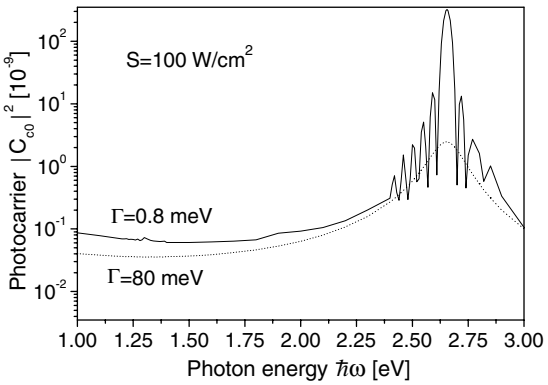

Figure 5. Occupation of the conduction-band ground state by CW excitation when $t = \infty$.

By re-formatting equation (13) as

$$i\hbar \frac{dC_j}{dt} = \sum_{si} h^s_{ji} \exp\left[i(E_j - E_i - \hbar\omega_s + i\Gamma_{ji})t/\hbar\right] C_i \tag{20}$$

where the external field is written as $\sum_s h^s e^{-i\omega_s t}$, the steady-state solution up to the second order has the form of $C_j(t) = C_j^{(0)} + C_j^{(1)}(t) + C_j^{(2)}(t)$. Here $\hbar\gamma_{ji} = \Gamma_{ji}$. For $t \to \infty$,

$$\begin{aligned} C_j^{(1)}(\infty) &= \sum_{sk} \frac{h^s_{jk} C_k^{(0)}}{E_j - E_k - \hbar\omega_s + i\Gamma_{jk}} \\ C_j^{(2)}(\infty) &= \sum_{sitk} \left(\frac{1}{E_j - E_i - \hbar\omega_s + i\Gamma_{ji}} - \frac{1}{E_j - E_k - \hbar\omega_s - \hbar\omega_t + i\Gamma_{jk}} \right) \\ &\quad \times \frac{h^s_{ji} h^t_{ik} C_k^{(0)}}{E_i - E_k - \hbar\omega_s + i\Gamma_{ik}}. \end{aligned} \tag{21}$$

For single-beam excitation, $s = t$ in $C_j^{(2)}$ so that equation (19) is retrieved when the Γ s are negligibly small since the absorption coefficient is proportional to $|C_j(\infty)|^2$ and $h \propto \sqrt{S}$, see equation (13). Optical spectra of molecules are characterized by sharp lines, while for the CdS QDs having radii of 3.7 nm under investigation, as well as many other semiconductor nanosystems of interest, the full width at half maximum of the photoluminescence peak is of the order of tens of meV [6]. In this case, $C_j^{(2)}$ is insignificant and C_j is always dominated by $C_j^{(1)}$ unless the optical excitation power is very strong. Moreover, $C_j^{(2)}$ is observable normally only when $C_j^{(1)}$ is zero, i.e., $h^s_{jk} = 0$ while $h^s_{ji} \neq 0$ and $h^s_{ik} \neq 0$. For CdS QDs, E_p is finite for the inter-band transitions so that $C^{(1)}$ always dominates for optical transition between ground states of the conduction and valence bands. This is believed to be the major reason why the multiphoton processes in semiconductor QDs are so effective.

Figure 5 shows the occupation of the conduction-band ground state as a function of the photon energy. The quantum selection rules of optical transitions (section 2.2) are critical in determining the optical properties of molecules where separations between energy levels are large. It becomes much relaxed in semiconductor nanoscale QDs because of the small separation between energy levels, especially in the valence band (see figure 2). It is also due to the finite E_p for the inter-band transitions so that $C^{(1)}$ always dominates for optical transition between ground states of the conduction and valence bands. In addition, γ in equation (13) is normally large in a semiconductor system because of the large number of

energy relaxation processes as compared with the small molecules. We thus observe only about one order of magnitude difference in the one-photon and two-photon excitation in figure 5 when $\Gamma = 80$ meV, which is typical for II–V semiconductors.

The multiphoton excitation spectral range is very broad. From about 1.0 to 2.5 eV (i.e., the two-photon excitation range before the one-photon resonance peak), the calculated $|C_{c0}|^2$ is much larger than $|C_{c1}|^2$ so that the emission spectrum is expected to be dominated by the recombination of the ground-state exciton, which will be narrow and symmetric, and independent of excitation frequency because of the broad excitation spectral range. It was shown that the power of spontaneous emission [35]

$$P_{\text{emission}} = \frac{\mu_0 e^2 \omega_{n0}^2 E_p}{6 m_0 c} |C_{c0}|^2 \tag{22}$$

due to the recombination of the electron occupying E_{c0}. For an optical excitation of 100 W cm^{-2}, $|C_{c0}|^2 = 3.6 \times 10^{-11}$ when the excitation photon energy is 1.33 eV. $|C_{c0}|^2 = 2.5 \times 10^{-9}$ when $\hbar\omega = 2.65$ eV. The corresponding output emission powers are therefore 1.0×10^{-21} and 2.75×10^{-19} W, respectively, for two-photon and one-photon excitations.

We now discuss the relevant experiment of Robinson and Goldberg [56], where III–V semiconductor QDs, having a dot density of about 200 dots μm^{-2} with a diameter of 18–20 nm, were fabricated. Near-field scanning optical microscopy, where the near-field tip has a diameter of 150 nm, was used to excite a very small ensemble of QDs. For about 1 μW excitation power, about 1.4×10^3 W cm^{-2}, the luminescence intensity at 1.889 eV is about 35 counts s^{-1} in a cross-section of 0.2×0.2 μm^2, where there are about eight QDs. This gives us an average emission power of 1.3×10^{-18} W per QD. Notice the fact that the photoluminescence experiments of Robinson and Goldberg use a higher optical excitation (higher than 1.995 eV) than the emission photon energies from quantum dots (from 1.8 to 1.925 eV), which is therefore classified a one-photon excitation.

When a linear relationship between the excitation and emission powers is assumed for semiconductor QDs, an emission power of 3.85×10^{-18} W is expected at a one-photon excitation of 1.4×10^3 W cm^{-2}, which is about three times larger than the III–V QDs of Robinson and Goldberg [56]. In addition, the relaxation energy in III–V material is normally only tens of meV so that a further enhanced emission power is expected.

Figure 5 clearly shows the need of pulsed lasers for effective multiphoton processes, where the occupation of the conduction-band states is very low at normal laser excitation, and the one-photon excitation is about two orders of magnitude higher than the two-photon excitation at the steady state ($t = \infty$). In the ultra-short period where an optical excitation is switched on at $t = 0$, situations become very different. Even when the excitation is weak, the two-photon process has the same order of magnitude as the one-photon excitation (figure 2). We model an ultrashort pulse from a mode-locked laser by a sech^2 function in the form of S_0 sech$^2[(t-t_0)/\delta]$, $S_0 = 10$ GW cm^{-2}, $t_0 = 500$ and $\delta t = 50$ fs. Figure 6 shows the significant occupation of the conduction-band ground state when the QD is two-photon optically excited and a strong emission from the QDs is thereafter expected. As a comparison, the photocarrier in the ground-state is getting to be saturated when one-photon excitation ($\hbar\omega = 2.6$ eV) is applied using the same laser pulse.

4. Summary

While the great majority of multiphoton studies are carried out with molecular chromophores, one has increasingly become aware of the intriguing possibilities offered by semiconductor quantum dots for multiphoton bioimaging owing to their outstanding properties. However, although some experimental studies have indeed been carried out, the study of design principles

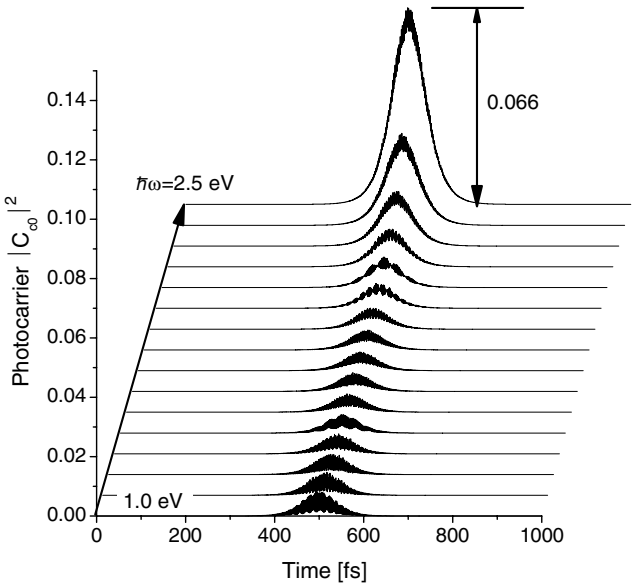

Figure 6. Temporal development of the conduction-band-ground-state photocarrier induced by a laser pulse. The arrow indicates the increase of the excitation photon energy from 1.0 to 2.6 eV. Notice that the energy separation between the two ground states in the conduction and valence bands is 2.67 eV.

as well as basic theory for their properties has been very limited. With this paper, multiphoton optical processes in semiconductor quantum dots (QDs) excited by ultra-fast (fs) and ultra-intense (GW cm^{-2}) lasers have been studied by solving the time-dependent Schrödinger equation nonperturbatively. This corresponds to a situation where conventional steady-state perturbation theory completely fails. It has been found that experimentally observed strong multiphoton excitations can be reproduced only when optical transitions among all confined states in the QD and an additional few hundred extended states in the barrier are taken into account in the numerical studies. Model calculations for a CdS QD of 3.7 nm in radius show that significant occupation of the conduction-band ground state can be excited by a 100 fs pulsed laser with a 10 GW cm^{-2} peak optical power and that the excitation rate is almost constant in the fundamental photon wavelength range from 1300 to 560 nm, which is a favourable region for bioimaging. With a working theory at hand, we are now in the position to explore design principles for QDs with optimum multiphoton excitation. We believe that our contribution will have a great impact on the biological community, and that it will be followed by many specific investigations aiming at optimal laser/quantum dot design for various measurement circumstances.

Acknowledgments

This work is supported by the Swedish Strategic Research Council (SSF) though a grant for research collaboration with Zhejiang University, China, within biophotonics.

References

[1] So P T C, Dong C Y, Masters B R and Berland K M 2000 Two-photon excitation fluorescence microscopy *Annu. Rev. Biomed. Eng.* **2** 399–429

[2] Zipfel W R, Williams R M and Webb W W 2003 Nonlinear magic: multiphoton microscopy in the biosciences *Nat. Biotechnol.* **21** 1369–77

[3] Jung J C, Mehta A D, Aksay E, Stepnoski R and Schnitzer M J 2004 *In vivo* mammalian brain imaging using one- and two-photon fluorescence microendoscopy *J. Neurophysiol.* **92** 3121–33
[4] Peng X, Manna L, Yang W, Wickham J, Scher E, Kadavanich A and Alivisatos A P 2000 Shape control of CdSe nanocrystals *Nature* **404** 59–61
[5] Gerion D, Pinaud F, Williams S C, Parak W J, Zanchet D, Weiss S and Alivisatos A P 2001 Synthesis and properties of biocompatible water-soluble silica-coated CdSe/ZnS semiconductor quantum dots *J. Phys. Chem.* B **105** 8861–71
[6] Michalet X, Pinaud F F, Bentolila L A, Tsay J M, Doose S, Li J J, Sundaresan G, Wu A M, Gambhir S S and Weiss S 2005 Quantum dots for live cells, *in vivo* imaging, and diagnostics *Science* **307** 538–44
[7] Larson D R, Zipfel W R, Williams R M, Clark S W, Bruchez M P, Wise F W and Webb W W 2003 Water-soluble quantum dots for multiphoton fluorescence imaging *in vivo Science* **300** 1434–6
[8] Lami J-F, Gilliot P and Hirlimann C 1996 Observation of interband two-photon absorption saturation in CdS *Phys. Rev. Lett.* **77** 1632–5
[9] Goeppert Mayer M 1931 Elementary processes with two quantum jumps *Ann. Phys., Lpz.* **9** 273–94
[10] Kaiser W and Garrett C G B 1961 Two-photon excitation in CaF_2:Eu^{2+} *Phys. Rev. Lett.* **7** 229–31
[11] Wherrett B S 1984 Scaling rules for multiphoton interband absorption in semiconductors *J. Opt. Soc. Am.* B **1** 67–72
[12] Schmidt M E, Blanton S A, Hines M A and Guyot-Sionnest P 1996 Size-dependent two-photon excitation spectroscopy of CdSe nanocrystals *Phys. Rev.* B **53** 12629–32
[13] Blanton S A, Dehesitani A, Lin P C and Guyot-Sionnest P 1994 Photoluminescence of single semiconductor nanocrystallites by two-photon excitation microscopy *Chem. Phys. Lett.* **229** 317–22
[14] Klimov V and McBranch D W 1998 Femtosecond high-sensitivity, chirp-free transient absorption spectroscopy using kilohertz lasers *Opt. Lett.* **23** 277–9
[15] Klimov V and McBranch D W 1998 Femtosecond 1P-to-1S electron relaxation in strongly confined semiconductor nanocrystals *Phys. Rev. Lett.* **80** 4028(4)
[16] Efros Al L and Efros A L 1982 Interband absorption of light in a semiconductor sphere *Sov. Phys.—Semicond.* **16** 772–5
[17] Brus L E 1984 Electron–electron and electron–hole interactions in small semiconductor crystallites: the size dependence of the lowest excited electronic state *J. Chem. Phys.* **80** 4403–9
[18] Kayanuma Y 1986 Wannier exciton in microcrystals *Solid State Commun.* **59** 405–8
[19] Schmidt H M and Weller H 1986 Quantum size effects in semiconductor crystallites: calculation of the energy spectrum for the confined exciton *Chem. Phys. Lett.* **129** 615–8
[20] Nair S V, Sinha S and Rustagi K C 1987 Quantum size effects in spherical semiconductor microcrystals *Phys. Rev.* B **35** 4098–101
[21] Kayanuma Y and Momiji H 1990 Incomplete confinement of electrons and holes in microcrystals *Phys. Rev.* B **41** 10261–3
[22] Madelung O (ed) 1992 *Data in Science and Technology: Semiconductors Other than Group IV Elements and III–V Compounds* (Boston, MA: Springer)
[23] Lawaetz P 1971 Valence-band parameters in cubic semiconductors *Phys. Rev.* B **4** 3460–7
[24] Lippens P E and Lannoo M 1990 Comparison between calculated and experimental values of the lowest excited electronic state of small CdSe crystallites *Phys. Rev.* B **41** 6079–81
[25] Lippens P E and Lannoo M 1989 Calculation of the band gap for small CdS and ZnS crystallites *Phys. Rev.* B **39** 10935–42
[26] Grabovskis V Ya, Dzenis Ya Ya, Ekimov A I, Kudryavtsev I A, Tolstoi M N and Rogulis U T 1989 Photoionization of semiconducting microcrystals in glass [luminescence studies] *Fiz. Tverd. Tela* **31** 272–5
Grabovskis V Ya, Dzenis Ya Ya, Ekimov A I, Kudryavtsev I A, Tolstoi M N and Rogulis U T 1989 *Sov. Phys.—Solid State* **31** 149–51 (Engl. Transl.)
[27] Swank R K 1967 Surface properties of II–VI compounds *Phys. Rev.* **153** 844–9
[28] Bujatti M 1968 CdS–metal barriers from photovoltage measurements *Br. J. Appl. Phys., J. Phys. D* **1** (ser.2) 581–4
[29] Sapra S and Sarma D D 2004 Evolution of the electronic structure with size in II–VI semiconductor nanocrystals *Phys. Rev.* B **69** 125304(7)
[30] Einevoll G T 1992 Confinement of excitons in quantum dots *Phys. Rev.* B **45** 3410–7
[31] Nair S V, Ramaniah L M and Rustagi K C 1992 Electron states in a quantum dot in an effective-bond-orbital model *Phys. Rev.* B **45** 5969–79
[32] Kang K I, McGinnis B P, Sandalphon, Hu Y Z, Koch S W, Peyghambarian N, Mysyrowicz A, Liu L C and Risbid S H 1992 Confinement-induced valence-band mixing in CdS quantum dots observed by two-photon spectroscopy *Phys. Rev.* B **45** 3465–8

[33] Vogl P, Hjalmarson H P and Dow J D 1983 A semi-empirical tight-binding theory of the electronic structure of semiconductor *J. Phys. Chem. Solids* **44** 365–78
[34] Sapra S, Shanthi N and Sarma D D 2002 Realistic tight-binding model for the electronic structure of II–VI semiconductors *Phys. Rev.* B **66** 205202(8)
[35] Fu Y, Luo Y and Ågren H 2006 Multiple-photon spectrum of CdS semiconductor quantum dot for bioimaging *Thin Solid Films* at press
[36] Merzbacher E 1998 *Quantum Mechanics* 3rd edn (New York: Wiley) pp 482–534
[37] Honig B, Jortner J and Szöke A 1967 Theoretical studies of two-photon absorption processes. I. Molecular benzene *J. Chem. Phys.* **46** 2714–27
[38] Mahr H 1975 *Quantum Electronics* vol 1 *Nonlinear Optics, Part A* ed H Rabin and C L Tang (New York: Academic) chapter 4 (Two-Photon Absorption Spectroscopy) pp 285–361
[39] Ridley B K 1988 *Quantum Processes in Semiconductor* (Oxford: Clarendon) p 185
[40] Fu Y and Willander M 1999 *Physical Models of Semiconductor Quantum Devices* (Boston, MA: Kluwer–Academic)
[41] Iannuzzi M and Polacco E 1964 Double-photon excitation of fluorescence in anthracene *Phys. Rev. Lett.* **13** 371–2
[42] Gold A and Hernandez J P 1965 One- and two-photon transitions of atoms in solids *Phys. Rev.* **139** A2002–7
[43] Liboff R L 2003 *Introductory Quantum Mechanics* 4th edn (San Francisco, CA: Addison Wesley) p 373
[44] Starace A F 1971 Length and velocity formulas in approximate oscillator-strength calculations *Phys. Rev.* A **3** 1242–5
[45] Pasquarello A and Quattropani A 1988 Gauge-invariant two-photon transitions in quantum wells *Phys. Rev.* B **38** 6206–10
[46] Lamb W E Jr and Retherford R C 1950 Fine structure of the hydrogen atom. Part I *Phys. Rev.* **79** 549–72
[47] Schlicher R R, Becker W, Bergou J and Scully M O 1984 Interaction Hamiltonian in quantum optics, or Ap versus rE revisited *Quantum Electrodynamics and Quantum Optics* ed A O Barut (New York: Plenum) pp 405–41
[48] Bauer D, Milosevic D B and Becker W 2005 Strong-field approximation for intense-laser-atom processes: the choice of gauge *Phys. Rev.* A **72** 023415(5)
[49] Haken H 1983 *Quantum Field Theory of Solids: An Introduction* (Amsterdam: North-Holland) p 312
[50] Bloembergen N and Shen Y R 1964 Quantum-theoretical comparison of nonlinear susceptibilities in parametric media, lasers, and Raman lasers *Phys. Rev.* **133** A37–49
[51] Ducuing J and Flytzanis C 1972 *Optical Properties of Solids* ed F Abelès (Amsterdam: North-Holland) chapter 11 (Second Order Optical Processes in Solids) pp 859–990
[52] van der Waerden B L 1932 *Die Gruppentheoretische Methode in der Quantenmechanik* (Berlin: Springer)
[53] Racah G 1942 Theory of complex spectra. II *Phys. Rev.* **62** 438–62
[54] Xu C and Webb W W 1996 Measurement of two-photon excitation cross sections of molecular fluorophores with data from 690 to 1050 nm *J. Opt. Soc. Am.* B **13** 481–91
[55] Sutherland R L 2003 *Handbook of Nonlinear Optics* 2nd edn (New York: Dekker) chapter 9 (Nonlinear Absorption) pp 579–626
[56] Robinson H D and Goldberg B B 2000 Light-induced spectral diffusion in single self-assembled quantum dots *Phys. Rev.* B **61** 5084(4)